Inorganic Chemistry

pubs.acs.org/IC

Article

Cation-Directed Synthetic Strategy Using 4f Tungstoantimonates as Nonlacunary Precursors for the Generation of 3d−4f Clusters

Elias Tanuhadi, Emir Al-Sayed, Ghenadie Novitchi, Alexander Roller, Gerald Giester, and Annette Rompel*

Cite This: *Inorg. Chem.* 2020, 59, 8461−8467

Read Online

ACCESS | Metrics & More | Article Recommendations | Supporting Information

ABSTRACT: The first synthetic pathway using a series of four nonlacunary 4f-heterometal-substituted polyoxotungstate clusters $Na_{21}[(Ln(H_2O)\text{-}(OH)_2(CH_3COO))_3(WO_4)(SbW_9O_{33})_3]\cdot nH_2O$ (**NaLnSbW$_9$**; Ln = Tb^{III}, Dy^{III}, Ho^{III}, Er^{III}, Y^{III}) as precursors for the directed preparation of nine new 3d−4f heterometallic tungstoantimonates $K_5Na_{12}H_3[TM(H_2O)\text{-}Ln_3(H_2O)_5(W_3O_{11})(SbW_9O_{33})_3]\cdot nH_2O$ (**KTMLnSbW$_9$**; TM = Co^{II}, Ni^{II}; Ln = Tb^{III}, Dy^{III}, Ho^{III}, Er^{III}, Y^{III}) has been developed. Systematic studies revealed an increased K content in the aqueous acidic reaction mixture to be the key step in the cation-directed preparation of 3d−4f compounds; among those, the Co-containing members represent the first examples of **KCoLnSbW$_9$** (Ln = Tb^{III}, Dy^{III}, Ho^{III}, Er^{III}, Y^{III}) heterometallic tungstoantimonates exhibiting the **SbW$_9$** building block. All 13 compounds have been characterized thoroughly in the solid state by powder and single-crystal X-ray diffraction (XRD), revealing a cyclic trimeric polyoxometalate architecture with three **SbW$_9$** units encapsulating a planar triangle of Ln^{III} ions in the case of **NaLnSbW$_9$** and a heterometallic core of one TM^{II} and three Ln^{III} for **KTMLnSbW$_9$** (TM = Co^{II}, Ni^{II}; Ln = Tb^{III}, Dy^{III}, Ho^{III}, Er^{III}, Y^{III}). The results obtained by XRD are supplemented by complementary characterization methods in the solid state such as IR spectroscopy, thermogravimetric analysis, and elemental analysis as well as in solution by UV−vis spectroscopy. Detailed magnetic studies on the representative compounds **KTMDySbW$_9$** (TM = Co^{II}, Ni^{II}) and **KCoYSbW$_9$** of the series revealed field-induced slow magnetic relaxation.

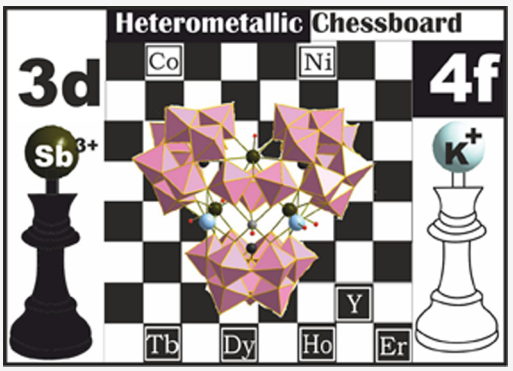

INTRODUCTION

Polyoxometalates (POMs)[1] are polyanions constructed of early-transition-state metals mostly in their highest oxidation states (V and VI), which are bridged by O atoms. Changing the size, shape, or composition of POMs enables their tuning for different kinds of applications ranging from catalysis,[2] materials science,[3] and molecular magnetism[4] to bio- and nanotechnology[5] as well as macromolecular crystallography.[6] Lacunary POMs have attracted significant attention in the past decades because they can be regarded as inorganic multidentate ligands toward electrophiles like transition metals (TMs) or lanthanides (Ln) to form more stable metal−oxo cluster structures.[7] While 3d-substituted POMs form the largest POM class and the field of 4f-containing POMs is significantly expanding at present, little has been reported on the field of heterometallic 3d−4f POMs[8,9] despite their interesting magnetic properties owing to the combination of 4f ions with large magnetic anisotropy exhibiting slow magnetic relaxation if coupled to 3d paramagnets[10] (Table S1).

This scarcity of 3d−4f heterometallic POM species can be explained by competitive reactions in the TM/Ln/POM systems, thereby most often resulting in only TM or Ln blocking the vacant sites of the cluster, leaving the remaining second metal type as a mere surface decoration.[10] As a matter of fact, a variety of different synthetic strategies have been developed to circumvent this problem.[11] For instance, the use of preformed 3d−4f metal complexes with labile ligands has been established by various working groups,[12] whereas the reaction of 3d-metal-substituted POM clusters with lanthanides to avoid the formation of pure 4f metal clusters has been applied as well.[13] However, the use of preformed 4f POM clusters as precursors for the preparation of 3d−4f clusters under mild conditions has not been reported yet, although such a synthetic approach may open new perspectives for the preparation of new 3d−4f-substituted POM compounds by shielding the overreactive 4f metal centers with multidentate lacunary ligands. Moreover, the use of preformed 4f-doped clusters as nonlacunary precursors[14] in combination with 3d

Received: March 25, 2020
Published: May 22, 2020

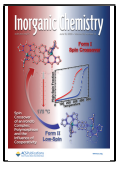

https://dx.doi.org/10.1021/acs.inorgchem.0c00890
Inorg. Chem. 2020, 59, 8461−8467

metals may facilitate the directed generation of high-nuclear POMs with a defined heterometallic core.

Herein, we report on the first step-by-step synthetic approach using four preformed high-nuclear 4f-doped tungstoantimonate clusters $Na_{21}[(Ln(H_2O)(OH)_2(CH_3COO))_3(WO_4)(SbW_9O_{33})_3]\cdot nH_2O$ (**NaLnSbW$_9$**) (Ln = Tb^{III}, Dy^{III}, Ho^{III}, Er^{III}, Y^{III}) as nonlacunary precursors to prepare a family of nine new 3d−4f heterometallic POM clusters $K_5Na_{12}H_3[TM(H_2O)Ln_3(H_2O)_5(W_3O_{11})(SbW_9O_{33})_3]\cdot nH_2O$ (**KTMLnSbW$_9$**; TM = Co^{II}, Ni^{II}; Ln = Tb^{III}, Dy^{III}, Ho^{III}, Er^{III}, Y^{III}; Table S2). Among those, the cobalt-substituted representatives **KCoLnSbW$_9$** (Ln = Tb^{III}, Dy^{III}, Ho^{III}, Er^{III}, Y^{III}) represent the first examples of heterometallic tungstoantimonates exhibiting the **SbW$_9$** building block. The versatility of the developed step-by-step protocol was probed by applying the synthetic conditions on the diamagnetic nonlacunary compound $Na_{16}(NH_4)[\{Y(\alpha\text{-}SbW_9O_{31}(OH)_2)(CH_3COO)(H_2O)\}_3(WO_4)]_3\cdot 48H_2O$ for the preparation of the isostructural $K_5Na_{12}H_3[Co(H_2O)Y_3(H_2O)_5(W_3O_{11})(SbW_9O_{33})_3]\cdot 46H_2O$ (**KCoYSbW$_9$**) eventually allowing for comparative magnetic studies on the Dy-containing representatives **KCoDySbW$_9$** and **KNiDySbW$_9$** of the heterometallic family.

RESULTS AND DISCUSSION

Synthesis. The first step in the preparation of the 3d−4f clusters was the synthesis of the nonlacunary 4f precursors. Among the Keggin-type polyoxotungstates (POTs), the trilacunary derivatives $\{XW_9O_{33}\}$ (X = As^{III}, Sb^{III}, Bi^{III})[15] represent ideal candidates for constructing POM-based metal clusters regarding their well-defined vacant sites and high negative charges.[16] Given the low reported number of only nine 3d−4f compounds based on the $Na_9[SbW_9O_{33}]\ 19.5H_2O$ $\{SbW_9O_{33}\}$ unit (Table S1) and the lone pair of the trilacunary precursor, which prevents the formation of a closed Keggin $\{XW_{12}O_{40}\}$ sphere, the $\{SbW_9O_{33}\}$ unit[15] was chosen as a building block. Initially, the 4f POT precursor was prepared upon the addition of the corresponding Ln salt to a solution of $\{SbW_9O_{33}\}$ in a 1:2 mixture of a H_2O/NaOAc buffer (pH 5.5, 2 M). In order to prevent the formation of insoluble lanthanide hydroxides, a low pH value in the range of 5.5 was combined with high acetate concentrations considering the templating effect of organic ligands, which temporarily coordinate to the Ln^{III} metal ions to decrease their overreactivity.[16]

For the second reaction step, a lower reaction temperature of 50 °C was chosen to ensure the integrity of the trimeric cluster. The corresponding TM was introduced as a chloride salt, $TMCl_2$ (TM = Ni^{II}, Co^{II}), together with a solution of K_2CO_3. As for the **KCoLnSbW$_9$** compounds, the addition of $CoCl_2$ to the reaction mixture instantaneously led to a pink solution, indicating the presence of octahedrally coordinated Co^{II} centers, whereas blue reaction solutions were observed at temperatures higher than 80 °C, which could be explained by the formation of square-pyramidally coordinated Co^{II} metal centers, as present in the Hervé-type sandwich POT.[17] Initial crystallization attempts upon slow evaporation of the reaction mixture in a pure NaOAc buffer resulted in three different crystal phases consisting of the desired 3d−4f cluster **KTMLnSbW$_9$**, unreacted 4f precursor, and the corresponding Krebs POM $Na_{10}[(TM(H_2O)_3)_2(WO_2)_2(SbW_9O_{33})_2]$ (TM = Co^{II}, Ni^{II}).[18] Regarding the 3:1 stoichiometric ratio of TM to 4f precursor, 1 equiv of TM was grafted onto the 3d−4f compound, whereas 2 equiv led to the formation of $Na_{10}[(TM(H_2O)_3)_2(WO_2)_2(SbW_9O_{33})_2]$, leaving the unreacted 4f precursor to crystallize (Figure S17). Single-crystal XRD studies on the crystal phases revealed K countercations originating from the added K_2CO_3 exclusively in the 3d−4f cluster (Scheme 1). Given the well-documented directing

Scheme 1. Schematic Representation of the Step-by-Step synthesis of KTMLnSbW$_9$ (TM = Co^{II}, Ni^{II}; Ln = Tb^{III}, Dy^{III}, Ho^{III}, Er^{III}, Y^{III})[a]

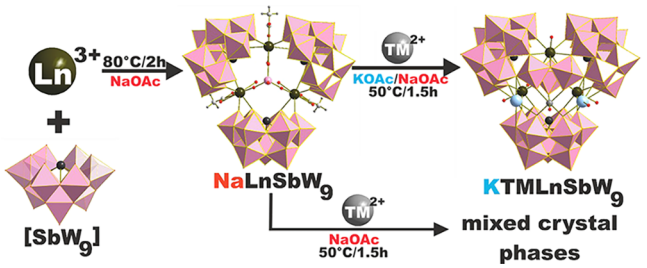

[a]The synthesis starts with the preparation of the 4f-doped compounds **NaLnSbW$_9$** upon the addition of Ln^{III} salts to a solution of **SbW$_9$** in an aqueous NaOAC buffer at 80 °C. Subsequent addition of the 3d metal salt TM^{II} to a 5% KOAc/NaOAc buffer (v/v) solution of **NaLnSbW$_9$** leads to the desired 3d−4f heterometallic clusters. Color legend: WO_6, fairy floss octahedra; Ln^{III}, dark-green balls; TM^{II}, gray balls; Sb^{III}, dark-gray balls; K^+, light-blue balls; O, red balls; C, white balls.

effect of countercations in POM reaction systems,[19] we chose to slightly increase the K content in the reaction mixture to favor formation and crystallization of the desired 3d−4f compounds. Initial attempts to increase the K content of the reaction mixture by merely adding KCl resulted in precipitates, which despite all our efforts could not be characterized. The appearance of insoluble precipitates upon the addition of KCl to the reaction mixture could be explained by a change of the ionic strength in the solution. As a matter of fact, the reaction medium was changed from pure NaOAc to a KOAc/NaOAc (5%, v/v) mixture, leading to an accelerated selective crystallization of the desired 3d−4f POM clusters by elevating the K content of the solution, while avoiding the introduction of further anions like chloride in the system and maintaining the initial pH value of 5.5. It should be mentioned that a one-pot synthetic approach by combining the corresponding 3d and 4f metals with the SbW_9 building block exclusively resulted in the formation of a Krebs POM.[20] Exchanging K with Cs as a countercation in an attempt to increase the product yield by further decreasing the solubility of the POM resulted in precipitates, which could not be identified. Despite all our efforts, single crystals of **KNiHoSbW$_9$** with sufficient quality for single-crystal XRD measurements could not be obtained. However, elemental analysis, IR spectroscopy, thermogravimetric analysis (TGA), and powder XRD measurements clearly indicate the successful synthesis of pure $K_5Na_{12}H_3[Ni(H_2O)Ho_3(H_2O)_5(W_3O_{11})(SbW_9O_{33})_3]\cdot 87H_2O$. To probe the versatility of the step-by-step synthesis protocol, the synthetic conditions were applied using the diamagnetic $Na_{16}(NH_4)[\{Y(\alpha\text{-}SbW_9O_{31}(OH)_2)(CH_3COO)(H_2O)\}_3(WO_4)]_3\cdot 48H_2O$[21] as a nonlacunary precursor in combination with Co^{II} ions, leading to the isolation of isostructural **KCoYSbW$_9$**. When this paper was under preparation, three crystal structures identical with our **NaLnSbW$_9$** (Ln = Dy^{III}, Ho^{III}, Er^{III}) 4f precursor have been

https://dx.doi.org/10.1021/acs.inorgchem.0c00890
Inorg. Chem. 2020, 59, 8461−8467

reported,[22] exhibiting a trimeric architecture composed of three trilacunary {SbW_9} units linked by three 8-coordinated Ln^{III} ions and a tetrahedral capping tungstate group, leading to a colloquial coined spinner with idealized C_{3v} symmetry. Note that for the synthesis of **$NaLnSbW_9$** different routes have been used by Cai et al. and our group. The structures reported by Cai et al. were synthesized at a neutral to slightly basic pH value of 7.2 with a {SbW_9}/Ln ratio of 1:2, whereas the synthesis protocol reported in this work applies a lower pH value of 5.5 and a {SbW_9}/Ln ratio of 1:1, which prevents the formation of insoluble lanthanide hydroxides, while using lower amounts of Ln salts, ultimately giving higher yields of 52−70% (this work) versus 18−25% based on Ln.[22]

Structure. Crystallographic studies on the in total 12 compounds showed that the four 4f precursors **$NaTbSbW_9$**, **$NaDySbW_9$**, **$NaHoSbW_9$**, and **$NaErSbW_9$** crystallize in the rhombohedral space group R_{3m}, whereas the 3d−4f polyanions **$KTMTbSbW_9$**, **$KTMDySbW_9$**, **$KCoHoSbW_9$**, **$KTMErSbW_9$**, and **$KCoYSbW_9$** (TM = Co^{II}, Ni^{II}) belong to the triclinic space group $P\bar{1}$. The Ln^{III} centers are arranged in a triangular shape with a Ln−Ln distance of 5.891 Å and a bond angle of 60°. Each Ln center exhibits a distorted square-antiprismatic coordination environment, with an acetate and a water ligand occupying the three peripheral positions of the metal centers and Ln−O bond lengths ranging from 2.20(3) to 2.43(2) Å (Figure S18 and Tables S4−S12).

For the 3d−4f counterparts, crystallographic studies showed a trimeric architecture composed of three {SbW_9} units, which are linked by a metal core comprising three 8-coordinated Ln^{III} metal centers connected to an octahedrally coordinated central W^{VI} position (Figure 1). The central W^{VI} unit is connected to two W^{VI} and a TM center (TM = Co^{II}, Ni^{II}), which act as capping moieties for the polyanion, resulting in an idealized C_{3v} symmetry. Each Ln^{III} exhibits a distorted square-antiprismatic coordination geometry. All three Ln centers are arranged in a triangular shape, with Ln−Ln distances ranging from 5.898 to 6.561 Å and an angle of 61.163°. The octahedrally coordinated TM center shows bond lengths from 1.957(19) to 2.083(16) Å, with a terminal water ligand occupying the free metal position (Figure 1 and Tables S13−S28). Powder XRD measurements were performed on the new compounds **$NaTbSbW_9$** (Figure S19) and **$KTMLnSbW_9$** (TM = Co^{II}, Ni^{II}; Ln = Tb^{III}, Dy^{III}, Ho^{III}, Er^{III}, Y^{III}; Figures S20 and S21) and compared to the corresponding simulated spectra, thereby showing the homogeneity of all bulk samples.

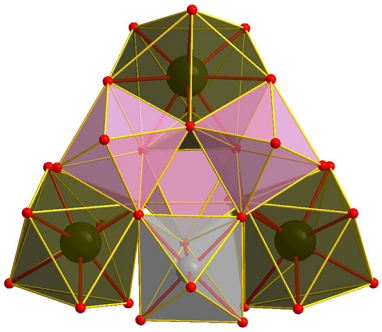

Figure 1. Polyhedral representation of the heterometallic core in **$KTMLnSbW_9$** (TM = Co^{II}, Ni^{II}; Ln = Tb^{III}, Dy^{III}, Ho^{III}, Er^{III}, Y^{III}). Color legend: WO_6, fairy floss octahedra; Ln, dark-green square-antiprismatic polyhedra; TM, gray octrahedron; O, red balls.

Besides XRD, all 13 compounds were characterized by attenuated-total-reflectance IR spectroscopy showing the terminal W=O and bridging W−O−W vibrations typical for the Keggin-type POT framework (Figures S1 and S2). The bands at 1541, 1460, and 1409 cm^{-1} are attributed to the stretching bands of the acetate−carboxylate groups, whereas a band belonging to the bending vibrations of the acetate methyl groups can be observed at 1348 cm^{-1} in **$NaLnSbW_9$** lacking in **$KTMLnSbW_9$** (Figure S3), which is in accordance to the crystal structures of the compounds.

The number of water molecules in the compounds $NaTbSbW_9{\cdot}71H_2O$ (Figure S4), $NaDySbW_9{\cdot}125H_2O$ (Figure S5), $NaHoSbW_9{\cdot}81H_2O$ (Figure S6), $NaErSbW_9{\cdot}96H_2O$ (Figure S7), $KNiTbSbW_9{\cdot}99H_2O$ (Figure S8), $KNiDySbW_9{\cdot}116H_2O$ (Figure S9), $KNiHoSbW_9{\cdot}87H_2O$ (Figure S10), $KNiErSbW_9{\cdot}69H_2O$ (Figure S11), $KCoTbSbW_9{\cdot}69H_2O$ (Figure S12), $KCoDySbW_9{\cdot}63H_2O$ (Figure S13), $KCoHoSbW_9{\cdot}61H_2O$ (Figure S14), $KCoErSbW_9{\cdot}70H_2O$ (Figure S15), and $KCoYSbW_9{\cdot}52H_2O$ (Figure S16) was determined using TGA (Table S3). All compounds exhibit, in general, two to four weight-loss regions that are attributed to losses of water and acetate ligands, respectively. The TGA spectra indicate no major decomposition up to 600 °C.

The UV−vis spectra of **$NaLnSbW_9$** (Figure S22) and **$KTMLnSbW_9$** (Figure S23) are characterized by an absorption maximum at 272 nm attributed to the $p_\pi(O_b) \rightarrow d_\pi^*(W)$ ligand-to-metal charge transfer typical for the Keggin-type framework.[23]

Magnetism. Information storage represents one of the most important uses of magnets nowadays. However, the superparamagnetic size, below which information cannot be permanently stored because magnetization freely fluctuates, poses a lower limit to the size of the memory elements.[24] This occurs at room temperature for particles in the range of 10−100 nm, owing to the nature of the material. A solution to this problem would be single-molecule magnets (SMMs) being molecules with slow relaxation of their magnetization. The combination of both 3d and 4f metal ions within a heterometallic core represents a promising approach in the preparation of SMMs because the 3d ions can provide significant spin (S), while 4f ions such as Dy^{III} contribute the anisotropy necessary to hinder spin inversion.[25] The magnetic behavior of the heterometallic Dy^{III}-containing members **$KCoDySbW_9$** and **$KNiDySbW_9$** was studied by measuring the direct-current (dc) and alternating-current (ac) magnetic properties of the compounds. To show the importance of the heterometallic core in the compounds, comparative magnetic studies were carried out on **$KCoYSbW_9$**.

The dc magnetic properties of the three representative compounds out of the reported series of POMs **$KCoDySbW_9$**, **$KNiDySbW_9$**, and **$KCoYSbW_9$** are shown in Figure 2 ($\chi_M T$ vs T plot). Magnetic measurements were carried out on microcrystalline powder samples between 2 and 300 K under an applied field of 1000 Oe. The $\chi_M T$ values are 45.06 and 44.74 cm^3 K mol^{-1} for **$KCoDySbW_9$** and **$KNiDySbW_9$**, respectively, at room temperature. These values are in good agreement with what is expected for three noninteracting Dy^{III} ions (14.17 cm^3 K mol^{-1}, $S = {}^5/_2$, $^6H_{15/2}$, $g = {}^4/_3$)[26] and one isolated Co^{II} or Ni^{II} ion (1.877 cm^3 K mol^{-1} and $g = 2$ for $S = {}^3/_2$ and 1.00 cm^3 K mol^{-1} and $g = 2$ for $S = 1$).[27] With decreasing temperature, the $\chi_M T$ products gradually decrease until $T = 2.0$ K and reach values of 35.98 and 37.27 cm^3K mol^{-1} for **$KCoDySbW_9$** and **$KNiDySbW_9$**, respectively, which

https://dx.doi.org/10.1021/acs.inorgchem.0c00890
Inorg. Chem. 2020, 59, 8461−8467

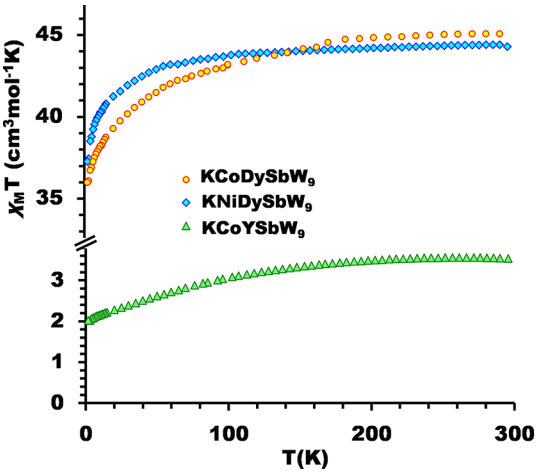

Figure 2. Temperature dependence of the $\chi_M T$ product at 1000 Oe for **KCoDySbW$_9$**, **KNiDySbW$_9$**, and **KCoYSbW$_9$**.

can be associated with the depopulation of MJ (Stark) sublevels of the Dy^{III} centers.[28] In the case of **KCoDySbW$_9$**, an additional contribution to decreasing the temperature dependence of magnetic susceptibility can be associated with the strong spin orbital component characteristic of octahedral Co^{II} ions.[27,29,30] This contribution is present in the heterometallic compound **KCoYSbW$_9$**, in which the strong paramagnetic ions are replaced by the diamagnetic yttrium(III) analogue. At room temperature, the $\chi_M T$ value for **KCoYSbW$_9$** is 3.54 cm^3 K mol^{-1} (Figure 2), which is significantly higher than the spin-only value for $S = {}^3/_2$ ($g = 2$). At 2 K, the product of $\chi_M T$ takes a value of 2.08 cm^3 K mol^{-1}. Low-temperature measurements (2 K) of the field dependence of magnetization exhibit near-saturation at 5 T, suggesting the presence of a well-isolated ground state in **KCoYSbW$_9$**. For **KCoDySbW$_9$** and **KNiDySbW$_9$**, the evolution of magnetization versus field has typical shapes and values, which correspond to the presence of three isolated Dy^{III} ions with significant magnetic anisotropy (Figure S29).[26,31]

The dynamic properties of compounds **KCoDySbW$_9$** (Figure S24), **KNiDySbW$_9$** (Figure S26), and **KCoYSbW$_9$** (Figure S25) were studied by measuring the temperature- and field-dependent ac magnetic susceptibility (Figures 3 and 4). For **KCoYSbW$_9$**, no signal was observed under zero dc field at

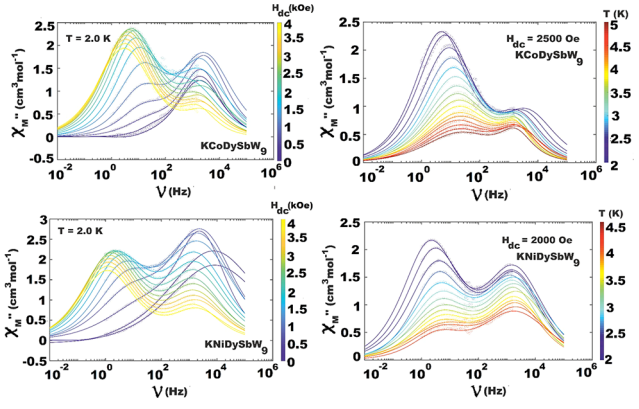

Figure 3. Frequency dependence of the out-of-phase susceptibility χ_M'' showing the two-relaxation processes of **KCoDySbW$_9$** and **KNiDySbW$_9$**.

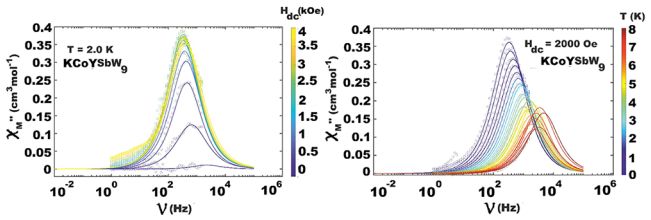

Figure 4. Frequency dependence of the out-of-phase susceptibility χ_M'' for **KCoYSbW$_9$**.

2.0 K in the out-of-phase component (χ_{ac}'') ac susceptibility. After the application of small dc fields (up to 4000 Oe), a frequency-dependent out-of-phase signal becomes visible (Figure S25A,B). Such behavior can be a consequence of the suppression of quantum tunneling of magnetization (QTM), indicating the presence of field-induced slow magnetic relaxation. The intensity of the out-of-phase signal gradually increases until about 2000 Oe and remains stable. To investigate the nature of this slow magnetic relaxation, the ac susceptibility data were collected under a fixed dc field and stable temperatures between 2.0 and 7.0 K (with a 0.2 K increment; Figure S25D,E). Evaluation of the field and temperature dependence of relaxation times was achieved by fitting the out-of-phase (χ_{ac}''; eq S3) and in-phase (χ_{ac}'; eq S2) components of the ac susceptibility using a generalized Debye model for a one-relaxation process.[32,33]

The dynamic properties of **KCoDySbW$_9$** and **KNiDySbW$_9$** are similar. At 2.0 K under zero dc field, a signal without a maximum was detected in the out-of-phase component of the ac susceptibility. With a change in the magnetic field, a clear maximum appears after 1500 Oe in the out-of-phase component of the ac susceptibility. The 2500 and 2000 Oe static fields were chosen for the temperature-dependent measurements (Figures S24D,E and S26D,E). Considering the shapes of the Cole−Cole plots derived from the temperature- and field-dependent measurements (Figures S24C,F and S26C,F), a two-step relaxation process is suggested for **KCoDySbW$_9$** and **KNiDySbW$_9$** and the ac susceptibility data were fitted with generalized Debye equations including a two-step relaxation process (eqs S4 and S5).[34] The two relaxation times (τ_1 and τ_2) and distribution parameters (α_1 and α_2) occur along with two isothermal susceptibilities (χ_{T1} and χ_{T2}) and one common adiabatic susceptibility (χ_s; eqs S4 and S5). In both compounds, the first relaxation process at low frequency (LF) is well-defined, while the second one at high frequency (HF) has large uncertainty estimates on variable parameters. The distributions of relaxation times for the LF relaxation process is rather broad ($\alpha_1 = 0.3–0.5$) but well-defined. This is most likely related to the presence of three crystallographically different Dy^{III} ions in the molecular structure (Figure 1), which can exhibit slightly different relaxation properties.

In the case of **KCoYSbW$_9$**, three different mechanisms of relaxation, namely, QTM, direct, and Raman or Orbach mechanisms, respectively, are suggested (Figure 5). It should be mentioned that the presence of either a Raman or Orbach mechanism, together with QTM and direct mechanisms of relaxation, is sufficient in order to obtain a satisfactory fit of data. For compounds **KCoDySbW$_9$** and **KNiDySbW$_9$**, only the LF signals were analyzed because the second process is poorly defined. In both compounds, QTM is well-defined and indispensable for fitting relaxation data of the LF signal. The

https://dx.doi.org/10.1021/acs.inorgchem.0c00890
Inorg. Chem. 2020, 59, 8461−8467

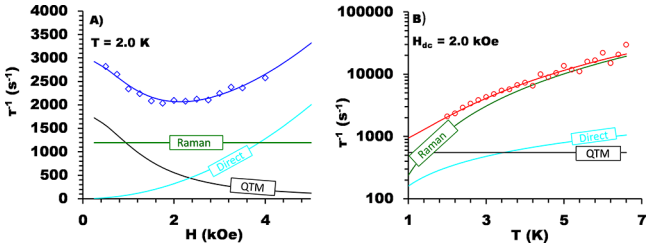

Figure 5. Field (A) and temperature (B) dependence of relaxation times (Table S29) based on eq S1 for **KCoYSbW$_9$**.

second mechanism may be Raman or Orbach with a satisfactory agreement factor (*R*; Table S29 and Figures S27 and S28).

CONCLUSIONS

In summary, a facile synthetic protocol for the directed step-by-step preparation of a 3d−4f heterometallic series of tungstoantimonates via preformed high-nuclear 4f-doped POMs as nonlacunary precursors is reported for the first time. Systematic studies on the reaction system revealed increased K contents as a key step in the directed preparation and isolation of pure **KTMLnSbW$_9$**. The compounds have been characterized thoroughly both in the solid state by single-crystal and powder XRD, IR spectroscopy, TGA, and elemental analysis as well as in solution by UV−vis spectroscopy. The versatility of the step-by-step protocol was shown by the successful preparation and characterization of isostructural compound **KCoYSbW$_9$** upon application of the synthetic conditions discussed in this work on the literature-known diamagnetic Y-containing compound. Variable-temperature and variable-field ac susceptibility measurements show that the Dy^{III}-containing representatives of the compound family exhibit field-induced slow magnetic relaxation, which is supplemented by comparative studies on isostructural **KCoYSbW$_9$** lacking the strong paramagnetic Dy^{III} centers. This work shows the importance of the countercations in solution and represents a first step toward the directed preparation of 3d−4f heterometallic POM clusters of a defined composition for magnetic studies by using preformed 4f tungstoantimonates as nonlacunary precursors.

ASSOCIATED CONTENT

Supporting Information

The Supporting Information is available free of charge at https://pubs.acs.org/doi/10.1021/acs.inorgchem.0c00890.

Details on the synthesis, IR, TGA, XRD, UV−vis, and magnetic studies (PDF)

Accession Codes

CCDC 1978889−1978900 contain the supplementary crystallographic data for this paper. These data can be obtained free of charge via www.ccdc.cam.ac.uk/data_request/cif, or by emailing data_request@ccdc.cam.ac.uk, or by contacting The Cambridge Crystallographic Data Centre, 12 Union Road, Cambridge CB2 1EZ, UK; fax: +44 1223 336033.

AUTHOR INFORMATION

Corresponding Author

Annette Rompel − *Fakultät für Chemie, Institut für Biophysikalische Chemie, Universität Wien, 1090 Wien, Austria;* orcid.org/0000-0002-5919-0553; Email: annette.rompel@univie.ac.at; https://www.bpc.univie.ac.at

Authors

Elias Tanuhadi − *Fakultät für Chemie, Institut für Biophysikalische Chemie, Universität Wien, 1090 Wien, Austria*

Emir Al-Sayed − *Fakultät für Chemie, Institut für Biophysikalische Chemie, Universität Wien, 1090 Wien, Austria*

Ghenadie Novitchi − *Laboratoire National des Champs Magnetiques Intenses, CNRS, 38042 Grenoble Cedex 9, France;* orcid.org/0000-0002-6109-6937

Alexander Roller − *Fakultät für Chemie, Zentrum für Röntgenstrukturanalyse, Universität Wien, 1090 Wien, Austria*

Gerald Giester − *Fakultät für Geowissenschaften, Geographie und Astronomie, Institut für Mineralogie und Kristallographie, Universität Wien, 1090 Wien, Austria*

Complete contact information is available at: https://pubs.acs.org/10.1021/acs.inorgchem.0c00890

Notes

The authors declare no competing financial interest.

ACKNOWLEDGMENTS

We gratefully acknowledge financial support from the Austrian Science Fund FWF (Grants P27534 and P33089) and University of Vienna for awarding a Uni:docs fellowship to E.T. We thank Ao.Univ.-Prof. Klaus Richter for support with powder XRD measurements and Ass.-Prof. Dr. Peter Unfried for TGA measurements. Last, the authors thank Nadiia Gumerova, Ph.D., for valuable discussions concerning this work.

REFERENCES

(1) Pope, M. T. *Heteropoly and Isopoly Oxometalates*; Springer-Verlag: Berlin, 1983; Vol. 2, pp 10−26.

(2) (a) Wang, S. S.; Yang, G. Y. Recent Advances in Polyoxometalate-Catalyzed Reactions. *Chem. Rev.* **2015**, *115* (11), 4893−4962. (b) Samaniyan, M.; Mirzaei, M.; Khajavian, R.; Eshtiagh-Hosseini, H.; Streb, C. Heterogeneous Catalysis by Polyoxometalates in Metal-Organic Frameworks. *ACS Catal.* **2019**, *9*, 10174−10191. (c) Liu, Z. J.; Wang, X. L.; Qin, C.; Zhang, Z. M.; Li, Y. G.; Chen, W. L.; Wang, E. B. Polyoxometalate-assisted synthesis of transition-metal cubane clusters as artificial mimics of the oxygen-evolving center of photosystem II. *Coord. Chem. Rev.* **2016**, *313*, 94−110.

(3) (a) Coronado, E.; Gomez-Garcia, C. J. Polyoxometalate-Based Molecular Materials. *Chem. Rev.* **1998**, *98*, 273−296. (b) Cherevan, A.; Nandan, S. P.; Roger, I.; Liu, R.; Streb, C.; Eder, D. Polyoxometalates on Functional Substrates: Concepts, Synergies, and Future Perspectives. *Adv. Sci.* **2020**, *7*, 1903511.

(4) (a) Ritchie, C.; Ferguson, A.; Nojiri, H.; Miras, H. N.; Song, Y.-F.; Long, D.-L.; Burkholder, E.; Murrie, M.; Kögerler, P.; Brechin, E. K.; Cronin, L. Polyoxometalate-Mediated Self-Assembly of Single-Molecule Magnets: $\{[XW_9O_{34}]_2[Mn^{III}_4Mn^{II}_2O_4(H_2O)_4]\}^{12-}$. *Angew. Chem., Int. Ed.* **2008**, *47*, 5609−5612. (b) Cardona-Serra, S.; Clemente-Juan, J. M.; Coronado, E.; Gaita-Ariño, A.; Camon, A.; Evangelisti, M.; Luis, F.; Martínez-Perez, M. J.; Sese, J. Lanthanoid Single-Ion Magnets Based on Polyoxometalates with a 5-fold Symmetry: The Series $[LnP_5W_{30}O_{110}]^{12-}$ (Ln^{3+} = Tb, Dy, Ho, Er, Tm, and Yb). *J. Am. Chem. Soc.* **2012**, *134*, 14982−14990. (c) Gumerova, N. I.; Roller, A.; Giester, G.; Krzystek, J.; Cano, J. A.; Rompel, A. Incorporation of Cr^{III} into a Keggin polyoxometalate as a chemical strategy to stabilize a labile $\{Cr^{III}O_4\}$ tetrahedral conformation and promote unattended single-ion magnet properties. *J. Am. Chem. Soc.* **2020**, *142*, 3336−3339. (d) Das, V.; Kaushik, R.; Hussain, F. Heterometallic 3d-4f polyoxometalates: An emerging field

with structural diversity to multiple applications. *Coord. Chem. Rev.* **2020**, *413* (15), 213271−213292.
(5) (a) Bijelic, A.; Aureliano, M.; Rompel, A. The antibacterial activity of polyoxometalates: structures, antibiotic effects and future perspectives. *Chem. Commun.* **2018**, *54*, 1153−1169. (b) Bijelic, A.; Aureliano, M.; Rompel, A. Polyoxometalates as Potential Next-Generation Metallodrugs in the Combat Against Cancer. *Angew. Chem.* **2019**, *131*, 3008−3029; *Angew. Chem., Int. Ed.* **2019**, *58*, 2980−2999. (c) Fraqueza, G.; Fuentes, J.; Krivosudský, L.; Dutta, S.; Mal, S. S.; Roller, A.; Giester, G.; Rompel, A.; Aureliano, M. Inhibition of Na^+/K^+- and Ca^{2+}-ATPase activities by phosphotetradecavanadate. *J. Inorg. Biochem.* **2019**, *197*, 110700.
(6) (a) Bijelic, A.; Rompel, A. The use of polyoxometalates in protein crystallography - An attempt to widen a well-known bottleneck. *Coord. Chem. Rev.* **2015**, *299*, 22−38. (b) Bijelic, A.; Rompel, A. Ten Good Reasons for the Use of the Tellurium-Centered Anderson-Evans Polyoxotungstate in Protein Crystallography. *Acc. Chem. Res.* **2017**, *50*, 1441−1448. (c) Bijelic, A.; Rompel, A. Polyoxometalates: more than a phasing tool in protein crystallography. *ChemTexts* **2018**, *4*, 10.
(7) (a) Ma, X.; Li, H.; Chen, L.; Zhao, J. The main progress over the past decade and future outlook on high-nuclear transition-metal substituted polyoxotungstates: from synthetic strategies, structural features to functional properties. *Dalton Trans.* **2016**, *45*, 4935−4960. (b) Hussain, F.; Gable, R. W.; Speldrich, M.; Kögerler, P.; Boskovic, C. Polyoxotungstate-encapsulated Gd_6 and Yb_{10} complexes. *Chem. Commun.* **2009**, *3*, 328−330.
(8) Zhao, K. W.; Li, Y.-Z.; Chen, L.-J.; Yang, G.-Y. Research progress on polyoxometalate-based transition-metal-rare-earth heterometallic derived materials: synthetic strategies, structural overview and functional application. *Chem. Commun.* **2016**, *52*, 4418−4445.
(9) Liu, J.; Han, Q.; Chen, L.; Zhao, J. A brief review of the crucial progress on heterometallic polyoxotungstates in the past decade. *CrystEngComm* **2016**, *18*, 842−862.
(10) Reinoso, S. Heterometallic 3d-4f polyoxometalates: still an incipient field. *Dalton Trans.* **2011**, *40*, 6610−6615.
(11) (a) Zhang, S.; Zhao, J.; Ma, P.; Chen, H.; Niu, J.; Wang, J. Organic-Inorganic Hybrids Based on Monovacant Keggin-type Silicotungstates and 3d-4f Heterometals. *Cryst. Growth Des.* **2012**, *12*, 1263−1272. (b) Gu, Y. N.; Chen, Y.; Wu, Y. L.; Zheng, S. T.; Li, X. X. A Series of Banana-Shaped 3d-4f Heterometallic Cluster Substituted Polyoxometalates: Syntheses, Crystal Structures, and Magnetic Properties. *Inorg. Chem.* **2018**, *57*, 2472−2479.
(12) (a) Fang, X.; Kögerler, P. A polyoxometalate-based manganese carboxylate cluster. *Chem. Commun.* **2008**, *29*, 3396−3398. (b) Fang, X.; Kögerler, P. PO_4^{3-}-Mediated Polyoxometalate Supercluster Assembly. *Angew. Chem., Int. Ed.* **2008**, *47*, 8123−8126.
(13) (a) Reinoso, S.; Galan-Mascaros, J. R. Heterometallic 3d-4f Polyoxometalate Derived from the Weakley-Type Dimeric Structure. *Inorg. Chem.* **2010**, *49*, 377−379. (b) Reinoso, S.; Galan-Mascaros, J. R.; Lezama, L. Heterometallic 3d-4f Polyoxometalate Derived from the Weakley-Type Dimeric Structure. *Inorg. Chem.* **2011**, *50*, 9587−9593.
(14) Tanuhadi, E.; Roller, A.; Kampatsikas, I.; Giester, G.; Rompel, A. Synthesis of the first Zn_6-hexagon sandwich-tungstoantimonate via rearrangement of a non-lacunary Krebs-type polyoxotungstate. *Dalton Trans.* **2018**, *47*, 15651−15655.
(15) (a) Tourne, C.; Revel, A.; Tourne, G.; Vendrell, M. C. R. Heteropolytungstates containing elements of phosphorus family with degree of oxidation (III) or (V)-identification of species having composition X_2W_{19} and XW_9 (X = P, As, Sb, Bi) and relation to those with composition XW11. *Acad. Sc. Paris, Ser. C* **1973**, *277*, 643−645. (b) Bösing, M.; Loose, I.; Pohlmann, H.; Krebs, B. New Strategies for the Generation of Large Heteropolymetalate Clusters: The β-B-SbW_9 Fragment as a Multifunctional Unit. *Chem. - Eur. J.* **1997**, *3*, 1232−1237. (c) Loose, I.; Droste, E.; Bösing, M.; Pohlmann, H.; Dickman, M. H.; Rosu, C.; Pope, M. T.; Krebs, B. Heteropolymetalate Clusters of the Subvalent Main Group Elements Bi^{III} and Sb^{III}. *Inorg. Chem.* **1999**, *38*, 2688−2694.
(16) Li, L.-L.; Han, H.-Y.; Wang, Y.-H.; Tan, H.-Q.; Zang, H. Y.; Li, Y.-G Construction of polyoxometalates from dynamic lacunary polyoxotungstate building blocks and lanthanide linkers. *Dalton Trans.* **2015**, *44*, 11429−11436.
(17) Tan, R.; Wang, C.; Cui, S.; Wang, H.; Han, J.; Xie, R. Synthesis, Crystal Structure and Antitumor Activities of a New Cobalt-containing Tungstoantimonate $Na_9[\{Na(H_2O)_2\}_3\{Co(H_2O)\}_3$ (α-B-$SbW_9O_{33})_2]\cdot 28\ H_2O$. *J. Macromol. Sci., Part A: Pure Appl.Chem.* **2014**, *51*, 33−36.
(18) Piepenbrink, M.; Limanski, E. M.; Krebs, B. Neue Heteropolyanionen des $M_2X_2W_{20}$-Typs mit Antimon(III) als Heteroatom. *Z. Anorg. Allg. Chem.* **2002**, *628*, 1187−1191.
(19) (a) Pradeep, C.; Long, D. L.; Cronin, L. Cations in control: crystal engineering polyoxometalate clusters using cation directed self-assembly. *Dalton Trans.* **2010**, *39*, 9443−9457. (b) Laronze, N.; Marrot, J.; Herve, G. Cation-Directed Synthesis of Tungstosilicates. 1. Syntheses and Structures of K_{10}A-α-$[SiW_9O_{34}]\eta\cdot 24\ H_2O$ of the Sandwich-Type Complex $K_{10.75}[Co(H_2O)_6]_{0.5}[Co(H_2O)_4Cl]_{0.25}$A-$\alpha$-$[K_2\{Co(H_2O)_2\}_3(SiW_9O_{34})_2]\cdot 32\ H_2O$ and of $Cs_{15}[K(SiW_{11}O_{39})_2]\cdot 39\ H_2O$. *Inorg. Chem.* **2003**, *42*, 5857−5862. (c) Misra, A.; Kozma, K.; Streb, C.; Nyman, M. Beyond Charge Balance: Counter-Cations in Polyoxometalate Chemistry. *Angew. Chem., Int. Ed.* **2020**, *59*, 596−612.
(20) Tanuhadi, E.; Kampatsikas, I.; Giester, G.; Rompel, A. Synthesis, characterization, and POM-protein interactions of a Fe-substituted Krebs-type Sandwich-tungstoantimonate. *Monatsh. Chem.* **2019**, *150*, 871−875.
(21) Ibrahim, M.; Mal, S. S.; Bassil, B. S.; Banerjee, A.; Kortz, U. Yttrium (III)-Containing Tungstoantimonate (III) Stabilized by Tetrahedral WO_4^{2-} Capping Unit, $[\{Y(\alpha\text{-}SbW_9O_{31}(OH)_2)\text{-}(CH_3COO)(H_2O)\}_3(WO_4)]^{17-}$. *Inorg. Chem.* **2011**, *50*, 956−960.
(22) Cai, J.; Ye, R.; Jia, K.; Qiao, X.; Zhao, L.; Liu, J.; Sun, W. pH-controlled construction of lanthanide clusters from lacunary polyoxometalate with single-molecule magnet behavior. *Inorg. Chem. Commun.* **2020**, *112*, 107694.
(23) Bi, L.; Li, B.; Wu, L.; Bao, Y. Synthesis, characterization and crystal structure of a novel 2D network structure based on hexacopper(II) substituted tungstoantimonate. *Inorg. Chim. Acta* **2009**, *362*, 3309−3313.
(24) Christou, G.; Gatteschi, D.; Hendrickson, D. N.; Sessoli, R. Single-Molecule Magnets. *MRS Bull.* **2000**, *25* (11), 66−71.
(25) Guo, Y. N.; Xu, G. F.; Guo, Y.; Tang, J. Relaxation dynamics of dysprosium (III) single molecule magnets. *Dalton Trans.* **2011**, *40*, 9953−9963.
(26) Benelli, C.; Gatteschi, D. Magnetism of Lanthanides in Molecular Materials with Transition-Metal Ions and Organic Radicals. *Chem. Rev.* **2002**, *102*, 2369−2388.
(27) Kahn, O. *Molecular Magnetism*; VCH Publishers, 1993.
(28) Kahn, M. L.; Ballou, R.; Porcher, P.; Kahn, O.; Sutter, J. P. Analytical Determination of the {Ln-Aminoxyl Radical} Exchange Interaction Taking into Account Both the Ligand-Field Effect and the Spin-Orbit Coupling of the Lanthanide Ion (Ln = Dy^{III} and Ho^{III}). *Chem. - Eur. J.* **2002**, *8*, 525−531.
(29) Lloret, F.; Julve, M.; Cano, J.; Ruiz-García, R.; Pardo, E. Magnetic Properties of Six-Coordinated High-Spin Cobalt (II) Complexes: Theoretical Background and Its Application. *Inorg. Chim. Acta* **2008**, *361*, 3432−3445.
(30) Titiš, J.; Boča, R. Magnetostructural D Correlations in Hexacoordinated Cobalt (II) Complexes. *Inorg. Chem.* **2011**, *50*, 11838−11845.
(31) Sorace, L.; Benelli, C.; Gatteschi, D. Lanthanides in Molecular Magnetism: Old Tools in a New Field. *Chem. Soc. Rev.* **2011**, *40*, 3092−3104.
(32) Gatteschi, D.; Sessoli, R.; Villain, J. *Molecular Nanomagnets*; Oxford University Press: Oxford, U.K., 2006; Vol. *1*, p 376.
(33) Amjad, A.; Figuerola, A.; Caneschi, A.; Sorace, L. Multiple Magnetization Reversal Channels Observed in a 3d-4f Single Molecule Magnet. *Magnetochemistry* **2016**, *2*, 27.

https://dx.doi.org/10.1021/acs.inorgchem.0c00890
Inorg. Chem. 2020, 59, 8461−8467

(34) Guo, Y.-N.; Xu, G.-F.; Gamez, P.; Zhao, L.; Lin, S.-Y.; Deng, R.; Tang, J.; Zhang, H.-J. Two-Step Relaxation in a Linear Tetranuclear Dysprosium (III) Aggregate Showing Single-Molecule Magnet Behavior. *J. Am. Chem. Soc.* **2010**, *132*, 8538−8539.

https://dx.doi.org/10.1021/acs.inorgchem.0c00890
Inorg. Chem. 2020, 59, 8461−8467